

Geocarto International

Publication details, including instructions for authors and
subscription information:

<http://www.tandfonline.com/loi/tgei20>

Applying six classifiers to airborne hyperspectral imagery for detecting giant reed

Chenghai Yang ^a, John A. Goolsby ^a, James H. Everitt ^a & Qian Du ^b

^a USDA-ARS, Kika de la Garza Subtropical Agricultural Research
Center, Weslaco, TX, 78596, USA

^b Department of Electrical and Computer Engineering, Mississippi
State University, Mississippi State, MS, 39762, USA

Accepted author version posted online: 25 Nov 2011. Version of
record first published: 04 Jan 2012

To cite this article: Chenghai Yang, John A. Goolsby, James H. Everitt & Qian Du (2012): Applying
six classifiers to airborne hyperspectral imagery for detecting giant reed, Geocarto International,
27:5, 413-424

To link to this article: <http://dx.doi.org/10.1080/10106049.2011.643321>

PLEASE SCROLL DOWN FOR ARTICLE

Full terms and conditions of use: <http://www.tandfonline.com/page/terms-and-conditions>

This article may be used for research, teaching, and private study purposes. Any
substantial or systematic reproduction, redistribution, reselling, loan, sub-licensing,
systematic supply, or distribution in any form to anyone is expressly forbidden.

The publisher does not give any warranty express or implied or make any representation
that the contents will be complete or accurate or up to date. The accuracy of any
instructions, formulae, and drug doses should be independently verified with primary
sources. The publisher shall not be liable for any loss, actions, claims, proceedings,
demand, or costs or damages whatsoever or howsoever caused arising directly or
indirectly in connection with or arising out of the use of this material.

Applying six classifiers to airborne hyperspectral imagery for detecting giant reed

Chenghai Yang^{a*}, John A. Goolsby^a, James H. Everitt^a and Qian Du^b

^aUSDA-ARS, Kika de la Garza Subtropical Agricultural Research Center, Weslaco, TX 78596, USA; ^bDepartment of Electrical and Computer Engineering, Mississippi State University, Mississippi State, MS 39762, USA

(Received 27 August 2011; final version received 18 November 2011)

This study evaluated and compared six image classifiers, including minimum distance (MD), Mahalanobis distance (MAHD), maximum likelihood (ML), spectral angle mapper (SAM), mixture tuned matched filtering (MTMF) and support vector machine (SVM), for detecting and mapping giant reed (*Arundo donax* L.), an invasive weed that presents a severe threat to agroecosystems throughout the southern US and northern Mexico. Airborne hyperspectral imagery was collected from a giant reed-infested site along the US-Mexican portion of the Rio Grande in 2009 and 2010. The imagery was transformed with minimum noise fraction (MNF) and the six classifiers were applied to the 30-band MNF imagery for each year. Accuracy assessment showed that SVM and ML generally performed better than the other four classifiers for overall classification and for distinguishing giant reed in both years. These results indicate that airborne hyperspectral imagery in conjunction with SVM and ML classification techniques is effective for detecting giant reed.

Keywords: maximum likelihood; mixture tuned matched filtering (MTMF); support vector machine (SVM); airborne hyperspectral imagery; giant reed

1. Introduction

Giant reed (*Arundo donax* L.) is a bamboo-like perennial grass that grows 3–10 m tall and spreads from horizontal rootstocks below the soil to form large colonies (Dudley 2000). It typically grows in riparian areas and floodplains and can be found on wet stream banks, gravel bars or dry banks away from permanent water (Newhouser *et al.* 1999). Currently, giant reed is an invasive weed throughout the southern half of the US and northern Mexico with the densest stands growing along the Rio Grande in Texas and the coastal rivers of southern California (Bell 1997, Everitt *et al.* 2004, Yang *et al.* 2011).

Giant reed consumes excessive amounts of water to supply its incredible rate of growth (Iverson 1994) and displaces native vegetation, leading to the destruction of wildlife habitats (Khudamrongsawat *et al.* 2004). Giant reed has become a major threat to riparian areas and watersheds in the Rio Grande Basin. Giant reed is also a major impediment to border patrol operations of the US Department of Homeland

*Corresponding author. Email: chenghai.yang@ars.usda.gov

Security's Customs and Border Protection along the international border between Laredo and Del Rio, TX, overrunning border access roads, reducing visibility and providing dense cover for illegal activities (Cleere 2007). The Department of Homeland Security officials have called for an immediate operational plan to control this invasive weed.

Accurate information on the spatial distribution and infested areas of giant reed is essential for effective management of this invasive weed. Remote sensing has the potential for providing timely and accurate information on the infestations of giant reed. Airborne multispectral imagery was evaluated for mapping giant reed infestations in Monterey County, California (Oakins 2001). Airborne visible infrared imaging spectrometer (AVIRIS) hyperspectral imagery was used for detecting and mapping giant reed in riparian areas in southern California (DiPietro *et al.* 2002). The light reflectance characteristics of giant reed were described and the application of aerial colour-infrared (CIR) photography and videography for detecting and mapping giant reed infestations in riparian areas in Texas was demonstrated (Everitt *et al.* 2004). More recently, high resolution satellite imagery has become available for remote sensing applications and provided new opportunities for effectively mapping invasive weeds. Both 2.8-m QuickBird and 10-m SPOT 5 satellite imagery have been evaluated for distinguishing giant reed infestations along the Rio Grande in southwest Texas (Everitt *et al.* 2005, 2008). The results showed that high resolution satellite imagery could be used to detect and map giant reed infestations as accurately as aerial photography and airborne multispectral imagery. As practical applications, 40 QuickBird images acquired between 2002 and 2007 from the Mexican portion of the Rio Grande Basin were used to estimate giant reed-infested areas and an estimated 4775 ha of giant reed existed along the major tributaries in the Mexican portion of the Basin (Yang *et al.* 2009b). Estimates based on aerial CIR photography taken in 2002 indicate that the portion of the Rio Grande from San Ygnacio to Lajitas, TX, a river length of 898 km, was infested with giant reed and that total giant reed area was 5981 ha (Yang *et al.* 2011).

Although aerial photography, airborne multispectral imagery and satellite imagery can be used successfully for mapping giant reed infestations, hyperspectral imagery that contains more spectral bands has the potential for more accurate classification in areas where there exist spectrally similar vegetation species to giant reed. Airborne hyperspectral imagery in conjunction with various image classification techniques has been evaluated for mapping a number of invasive weed species, including leafy spurge (*Euphorbia esula* L.) (Parker-Williams and Hunt 2002, Glenn *et al.* 2005), iceplant [*Carpobrotus edulis* (L.) N.E. Br] and jubata grass [*Cortaderia jubata* (Lem.) Stapf] (Underwood *et al.* 2003), hoary cress (*Lepidium draba* L.) (Mundt *et al.* 2005), waterhyacinth [*Eichhornia crassipes* (Mart.) Solms] (Yang and Everitt 2007), yellow starthistle (*Centaurea solstitialis* L.) (Miao *et al.* 2006), saltcedar (*Tamarix* sp. Lour.) (Narumalani *et al.* 2006, 2009), Ashe juniper (*Juniperus ashei* Buchholz) (Yang *et al.* 2009) and broom snakeweed [*Gutierrezia sarothrae* (Pursh.) Britt. and Rusby] (Yang and Everitt 2010). Currently, very limited research has been conducted on the use of hyperspectral imagery for detecting giant reed. As hyperspectral image data are becoming more available and less expensive, it is necessary to evaluate this type of image data and identify optimal classification methods for this application. Therefore, the objectives of this study were to evaluate airborne hyperspectral imagery and compare six commonly used classifiers, including minimum distance (MD), Mahalanobis distance (MAHD), maximum

likelihood (ML), spectral angle mapper (SAM), mixture tuned matched filtering (MTMF) and support vector machine (SVM), for distinguishing giant reed.

2. Methods

2.1 Study site

This study was conducted at a giant reed-infested area along the US-Mexico portion of Rio Grande near Quemado, TX. Giant reed grows in association with woody and herbaceous vegetation on both sides of the river. The longitude and latitude coordinates near the centre of the site are (100°38'38"W, 28°58'25"N).

2.2 Hyperspectral imagery acquisition

Hyperspectral imagery was acquired using an airborne imaging system described by Yang *et al.* (2003). The system consisted of a digital CCD camera, a hyperspectral filter, a front lens and a PC equipped with a frame grabbing board and camera utility software. The hyperspectral imaging system was configured to capture 12-bit images in 128 bands in the visible to NIR region of the spectrum (457–922 nm) with a bandwidth of 3.6 nm. The swath of images was 640 pixels.

A Cessna 206 single-engine aircraft with a camera port in the floor was used as the platform for image acquisition. No stabilizer or inertial measurement device was used to dampen or measure platform variations, but care was taken to minimize the effects of winds and changes in the aircraft's speed and flight direction. The aircraft was stabilized at a predetermined altitude of 2440 m above ground level, a speed of 180 km/h, and a flight direction during the course of image acquisition. A ground pixel size of approximately 2.0 m was achieved. Hyperspectral imagery was acquired between 1200 and 1400 h central standard time on 18 November 2009 and 8 October 2010 under sunny and calm conditions.

2.3 Image processing, transformation and classification

The geometric distortions due to movements in the across-track direction and variations in roll were corrected using a reference line approach (Yang *et al.* 2003). The geometrically corrected hyperspectral images were rectified to a georeferenced CIR image using rubber sheeting. The CIR image was taken using a multispectral imaging system and rectified to the universal transverse mercator (UTM), World Geodetic Survey 1984 (WGS-84), Zone 14N, coordinate system based on a set of the ground control points located with a submeter-accuracy Trimble GPS Pathfinder ProXRT receiver (Trimble Navigation Limited, Sunnyvale, CA). The procedure for image rectification was performed using ERDAS IMAGINE (ERDAS, Inc., Norcross, GA). Bands 1–5 and 108–128 (a total of 26 bands) appeared to be noisy and were removed from each hyperspectral image and the remaining 102 bands with a spectral range of 475–845 nm were used for analysis.

The minimum noise fraction (MNF) transformation implemented in ENvironment for Visualizing Images (ENVI) (Research Systems, Inc., Boulder, CO, USA) was used to reduce the spectral dimensionality and spectral noise in the hyperspectral imagery. The MNF transform is based on two principal component analysis transformations and divides the original hyperspectral data into two parts: one part associated with large eigenvalues and coherent eigenimages, and a complementary

part with near-unity eigenvalues and noise-dominated images (Green *et al.* 1988). Figure 1 shows eigenvalues of the first 50 MNF bands derived from the two hyperspectral images for the two years. Eigenvalues decrease sharply from about 240 for 2009 and from 190 for 2010 to about 2 at MNF band 20 for both years. Since bands with large eigenvalues contain useful data and bands with eigenvalues near one contain noise, the bands greater than 20 contained mainly noise. Based on the eigenvalue plots and visual inspection of the MNF band images, the first 20 bands from the transformed MNF images would be sufficient to replace the original 102-band images. For potential improvement on classification results, the first 30 bands from the MNF images were selected for image classification.

The major cover type classes for the study site consisted of giant reed, mixed woody and herbaceous vegetation, bare soil/roads and water. For 2009, giant reed included healthy giant reed and moisture-stressed giant reed with smaller and sparser stands. Because of the variations within the classes, each major class was divided into more subclasses. For 2009, there were a total of 11 subclasses, including four subclasses of giant reed, one class of moisture-stressed giant reed, three subclasses of mixed dense vegetation, two subclasses of bare soil and sparse vegetation and one class of water. For 2010, there were also a total of 11 subclasses, including three subclasses of giant reed, four subclasses of mixed dense vegetation, two subclasses of bare soil and sparse vegetation and two subclasses of water. For supervised training, different numbers of areas or regions of interest, with known cover types were selected and digitized on each image as the training samples to represent respective subclasses or endmembers. These training areas were first verified on the ground and then selected on the hyperspectral images as training samples. The numbers of digitized training pixels ranged from 288 to 1532 among the 11 subclasses for 2009

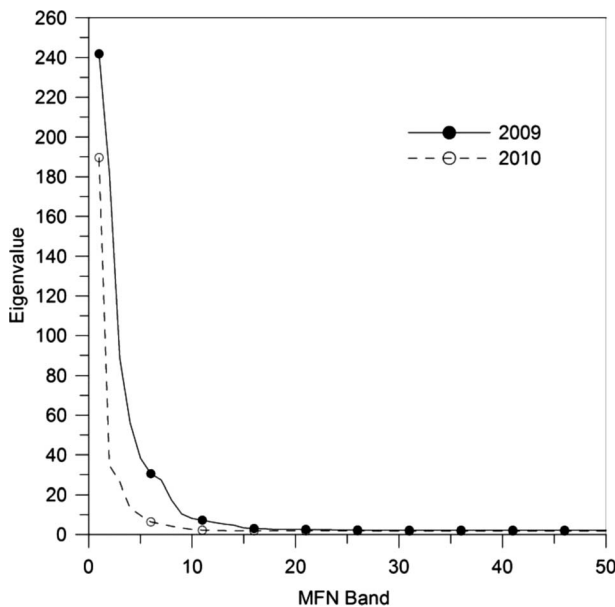


Figure 1. Minimum noise fraction (MNF) eigenvalues versus MNF bands derived from two 102-band hyperspectral images taken at a giant reed-infested site near Quemado, TX in 2009 and 2010, respectively.

and from 230 to 1194 among the 11 subclasses for 2010. A boundary was defined for the study site to exclude the areas outside the boundary for image classification. The total area encompassed by the boundary was approximately 57 ha.

Six commonly used supervised classification methods, including MD, MAHD, ML, SAM, MTMF and SVM, were applied to the two 30-band MNF images. The ML classifier uses the class means derived from the training data and assigns each pixel to the class that has the closest Euclidean distance from the pixel (ERDAS 2002). The MAHD method is similar to MD, except that the covariance matrix is used in the calculation (ERDAS 2002). Each pixel is assigned to the class for which MAHD is the smallest. ML classification assumes that the data for each class in each band are normally distributed and it calculates the probability that a given pixel belongs to a specific class (Richards 1999). Each pixel is assigned to the class that has the highest probability (i.e. the ML). SAM is a spectral classification technique that uses the n-dimensional angle to match pixels to endmembers (Kruse *et al.* 1993). The algorithm determines the spectral similarity between a pixel spectrum and an endmember spectrum by calculating the angle between them, treating them as vectors in a space with dimensionality equal to the number of bands. Each pixel is assigned to the endmember whose spectrum has the smallest spectral angle with the pixel spectrum. MTMF is a spectral unmixing technique that maximizes the response of the defined endmembers on each endmember abundance image (Harsanyi and Chang 1994). The matched filtering (MF) score images were then classified into the defined endmembers or subclasses based on maximum abundance values. In other words, each pixel was assigned to the class that had the highest MF score. The SVM classifier is a kernel-based machine learning technique that separates the classes with a decision surface that maximizes the margin between the classes (Hsu *et al.* 2007). Each pixel is classified to the class having the highest probability. There were six classification maps for each year. The subclasses within each classification map were then merged into the five defined major classes for 2009 and the four major classes for 2010.

2.4 Accuracy assessment

For accuracy assessment of the merged classification maps, 125 points were generated and assigned to the classes in a stratified random pattern for each year. The UTM coordinates of these points were determined and the Trimble GPS receiver was used to navigate to these points for ground verification. Error matrices for each classification map were generated by comparing the classified classes with the actual classes at these points. Overall accuracy, producer's accuracy, user's accuracy and kappa coefficients were calculated based on the error matrices. Kappa analysis was also performed to test if each classification was significantly better than a random classification and if any two classifications were significantly different (Congalton and Green 1999).

3. Results and discussion

Figure 2 shows two pairs of normal colour and CIR composite images derived from the two 102-band hyperspectral images acquired in 2009 and 2010, respectively. On the normal colour images, healthy giant reed has a smooth green colour, whereas other mixed dense vegetation has a dark green tone. On the CIR image, healthy giant

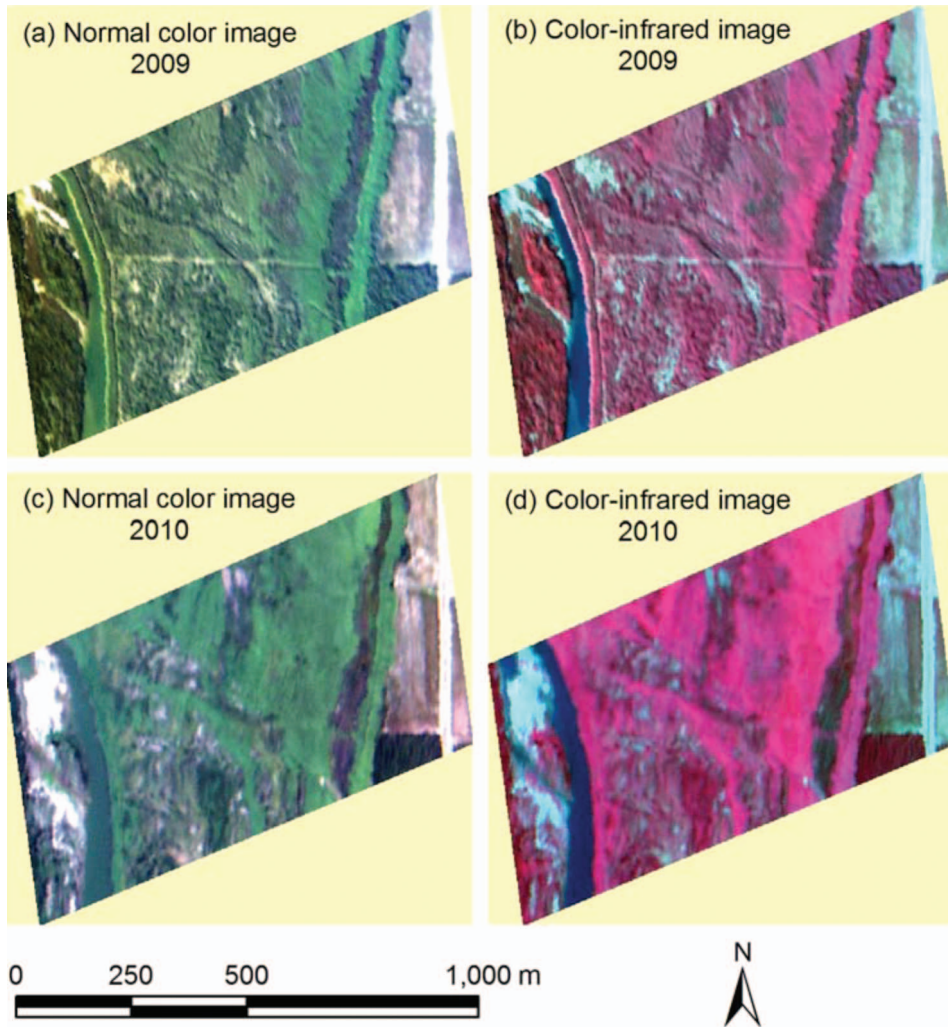


Figure 2. Normal colour and colour-infrared (CIR) composite images derived from two 102-band hyperspectral images taken at a giant reed-infested site near Quemado, TX in 2009 and 2010, respectively.

reed has a distinct bright reddish colour, though moisture-stressed giant reed in 2009 has a dark reddish tone. Mixed dense woody and herbaceous vegetation show a dark reddish tone with variations among different species, sparse senescing grass and herbaceous species have a greyish to pinkish response, bare soil and roads have a light grey to white colour, and water has a blue colour. Although healthy giant reed had a distinct spectral response, the stressed giant reed in 2009 had a similar spectral response to mixed vegetation species as shown on the normal colour and CIR images.

Figures 3 and 4 give the classification maps based on the ML and SVM classifiers for 2009 and 2010, respectively. Visual comparison of the classification maps with the normal and CIR images shown in Figure 2 indicates that giant reed and other cover types were well separated on the ML and SVM classification maps.

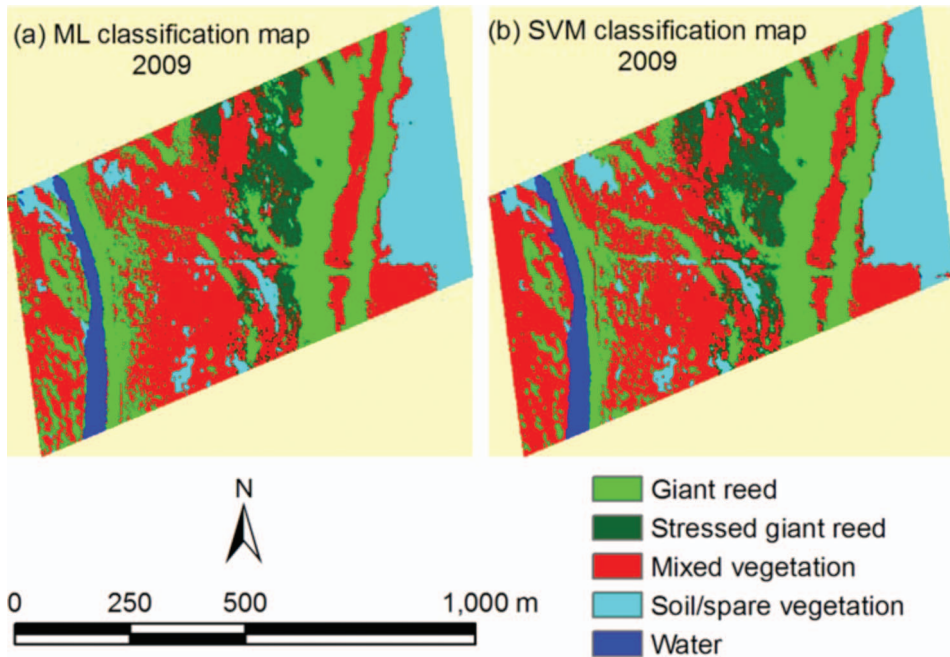


Figure 3. Five-category classification maps based on (a) maximum likelihood (ML) and support vector machine (SVM) classifiers from the 30-band minimum noise function (MNF) image transformed from a 102-band hyperspectral image for a giant reed-infested site near Quemado, TX in 2009.

To quantitatively evaluate the performance of the six classifiers, Table 1 summarizes the accuracy assessment results for the classification maps generated from the 30-band MNF images based on the six classifiers in 2009 and 2010. Overall, accuracy ranged from 88.0% to 94.4% in 2009 and from 88.0% to 95.2% in 2010. Among the six classifiers, SVM had the highest overall accuracy, whereas MTMF had the lowest overall accuracy in both years. Overall kappa varied from 0.835 to 0.27 for 2009 and from 0.824 to 0.929 for 2010 among the six classifiers, indicating the classification results agreed well with the reference data (a kappa value of 1 represents a perfect agreement between the classification and reference data). Kappa analysis showed that all the classifications were significantly better than a random classification.

Table 2 gives the kappa analysis results for pairwise comparisons among the six classification maps for each of the two years. For 2009, SVM was significantly better than MD, MAHD, SAM and MTMF, while ML performed as well as SVM. Moreover, ML was significantly better than SAM, but there were no significant differences among MD, MAHD and ML or among MD, MAHD, SAM and MTMF. For 2010, SVM was significantly better than MAHD, SAM and MTMF, while MD and ML performed equally well compared with SVM. However, there were no significant differences among MD, MAHD, ML, SAM and MTMF. These results indicate that SVM and ML generally performed better than the other classifiers for both years.

Tables 3 and 4 summarize the producer's and user's accuracies for the classification maps generated from the 30-band MNF images based on the six classifiers for 2009 and 2010, respectively. For 2009, SVM and ML provided

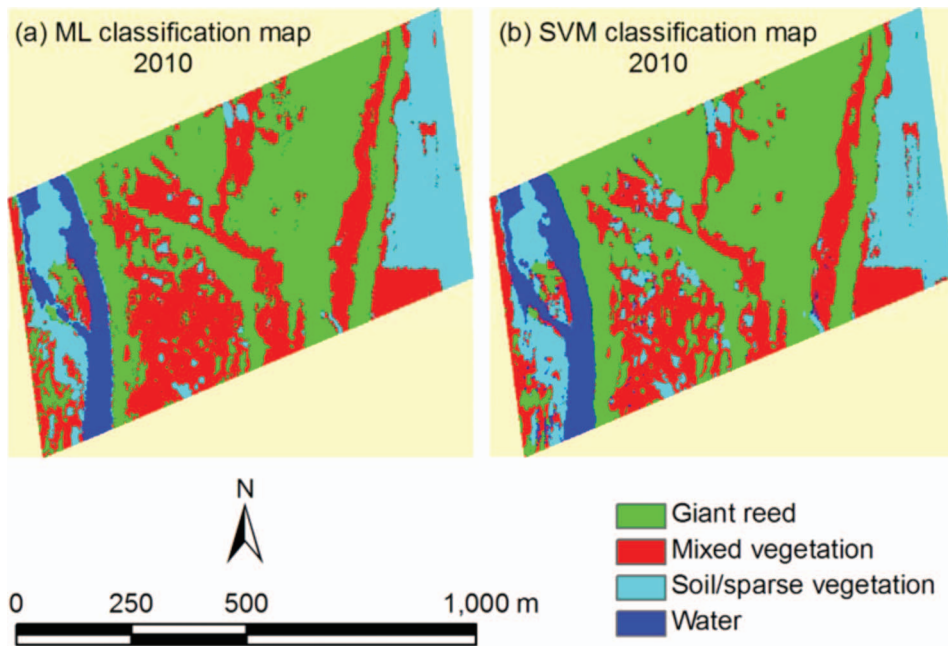


Figure 4. Five-category classification maps based on (a) maximum likelihood (ML) and (b) support vector machine (SVM) classifiers from the 30-band minimum noise function (MNF) image transformed from a 102-band hyperspectral image for a giant reed-infested site near Quemado, TX in 2010.

Table 1. Overall accuracy indicators for classification maps based on six classification methods from the 30-band minimum noise fraction (MNF) images transformed from two hyperspectral images for a giant reed-infested site near Quemado, TX in 2009 and 2010, respectively.

Classifier	2009			2010		
	Overall accuracy	Overall kappa	Z statistic*	Overall accuracy	Overall kappa	Z statistic*
MD	88.8	0.856	23.4	92.8	0.895	26.4
MAHD	88.8	0.855	23.3	89.6	0.849	21.4
ML	93.6	0.917	32.2	92.0	0.883	24.8
SAM	87.2	0.835	21.6	89.6	0.848	21.3
MTMF	88.0	0.844	22.3	88.0	0.824	19.3
SVM	94.4	0.927	34.7	95.2	0.929	33.0

Notes: MD, minimum distance; MAHD, Mahalanobis distance; ML, maximum likelihood; SAM, spectral angle mapper; MTMF, mixture tuned matched filtering; and SVM, support vector machine. *All classifications are significantly different from a random classification at the 0.05 level.

excellent producer's and user's accuracies ranging from 90.5 to 100% for both giant reed and stressed giant reed. MD and MTMF also had excellent producer's and user's accuracies from 91.2 to 96.9% for giant reed, but the user's accuracy for stressed giant reed was 72% for MD and 82.6% for MTMF. The lower user's accuracy was mainly due to the misclassification of mixed vegetation as stressed

Table 2. Kappa analysis results (Z-statistic) for pairwise comparisons among six classification maps generated from the 30-band MNF image transformed from two 102-band hyperspectral images taken at a giant reed-infested site near Quemado, TX in 2009 and 2010, respectively.

Classifier	MD	MAHD	ML	SAM	MTMF
Based on 2009 image					
MAHD	0.01				
ML	-1.33	-1.33	1.70*		
SAM	0.38	0.38	1.54	-0.17	-1.80*
MTMF	0.22	0.21	-0.27	-1.96*	
SVM	-1.59*	-1.59*			
Based on 2010 image					
MAHD	0.88				
ML	0.24	-0.64	0.65		
SAM	0.89	0.01	1.07	0.42	-2.07*
MTMF	1.31	0.43	-1.02	-1.66*	
SVM	-0.78	-1.65*			

Notes: MD, minimum distance; MAHD, Mahalanobis distance; ML, maximum likelihood; SAM, spectral angle mapper; MTMF, Mixture tuned matched filtering; and SVM, support vector machine. *Significantly different between the two classifications at the 0.05 level. The negative sign indicates that the classification method on the left is better than the one on the top.

Table 3. Accuracy assessment results for six classification maps generated from the 30-band minimum noise function (MNF) image transformed from a 102-band hyperspectral image of a giant reed-infested site near Quemado, TX in 2009.

Classifier	Overall accuracy (%)	Producer's accuracy (PA, %) and user's accuracy (UA, %)									
		Giant reed		Stressed giant reed		Mixed dense vegetation		Bare soil/sparse vegetation		Water	
		PA	UA	PA	UA	PA	UA	PA	UA	PA	UA
MD	88.8	91.2	93.9	90.0	72.0	80.0	84.8	92.3	100.0	100.0	100.0
MAHD	88.8	88.2	93.8	95.0	79.2	85.7	81.1	84.6	100.0	100.0	100.0
ML	93.6	94.1	94.1	95.0	90.5	91.4	88.9	92.3	100.0	100.0	100.0
SAM	87.2	88.2	93.8	95.0	73.1	74.3	78.8	92.3	100.0	100.0	100.0
MTMF	88.0	91.2	96.9	95.0	82.6	91.4	76.2	69.2	100.0	100.0	100.0
SVM	94.4	94.1	100.0	95.0	90.5	94.3	86.8	92.3	100.0	100.0	100.0

Note: MD, minimum distance; MAHD, Mahalanobis distance; ML, maximum likelihood; SAM, spectral angle mapper; MTMF, mixture tuned matched filtering; and SVM, support vector machine.

giant reed. MAHD and SAM provided accuracy values of 88.2–93.8% for giant reed and 79.2–95% for stressed giant reed. For 2010, SVM had a producer's accuracy of 93.3% and a user's accuracy of 100% for giant reed. The other five classifiers provided producer's accuracy values of 85–88.3% and user's accuracies of 94.6–100% for giant reed. The lower producer's accuracy values for all the classifiers were mainly caused by the misclassification of giant reed as mixed dense vegetation.

For mixed dense vegetation, SVM and ML provided producer's and user's accuracy values of 86.8–94.3% in 2009, whereas as the other four classifiers had accuracy values of 74.3–91.4% in the same year. SVM was also effective in distinguishing mixed dense vegetation in 2010 with a producer's accuracy of

Table 4. Accuracy assessment results for six classification maps generated from the 30-band minimum noise function (MNF) image transformed from a 102-band hyperspectral image of a giant reed-infested site near Quemado, TX in 2010.

Classifier	Overall accuracy (%)	Producer's accuracy (PA, %) and user's accuracy (UA, %)							
		Giant reed		Mixed dense vegetation		Bare soil/sparse vegetation		Water	
		PA	UA	PA	UA	PA	UA	PA	UA
MD	92.8	88.3	100.0	100.0	76.3	91.3	100.0	100.0	100.0
MAHD	89.6	85.0	100.0	96.6	70.0	87.0	95.2	100.0	100.0
ML	92.0	86.7	98.1	96.6	77.8	100.0	95.8	92.3	100.0
SAM	89.6	86.7	98.1	89.7	74.3	95.7	91.7	92.3	92.3
MTMF	88.0	88.3	94.6	75.9	78.6	100.0	79.3	92.3	100.0
SVM	95.2	93.3	100.0	96.6	84.8	95.7	95.7	100.0	100.0

Note: MD, minimum distance; MAHD, Mahalanobis distance; ML, maximum likelihood; SAM, spectral angle mapper; MTMF, mixture tuned matched filtering; and SVM, support vector machine.

96.6% and a user's accuracy of 84.8%. However, the other classifiers had lower user's accuracy values (70–78.6%) due to the misclassification of giant reed as mixed dense vegetation. For the bare soil and sparse vegetation category, MD, ML, SAM and SVM provided excellent results (92.3–100% in 2009 and 91.7–100% in 2010), while MAHD and MTMF had lower accuracy values in both years. As expected, water was the easiest cover type to distinguish. All the six classifiers accurately separated water with accuracy values of 100% in 2009 and 92.3–100% in 2010.

Based on the results of overall accuracy, producer's accuracy, user's accuracy and kappa analysis of all the classification maps for the two years, SVM appeared to be the best classifier. Although ML was not consistently superior to MD, MAHD, SAM and MTMF in all the cases, it provided excellent overall accuracy and more balanced producer's and user's accuracies for the individual classes, especially for giant reed and stressed giant reed. Nevertheless, the other four classifiers have the potential to be as effective as ML. Of the six classifiers evaluated in this study, MTMF is a subpixel or soft classifier, while the other five are hard classifiers. Due to the high spatial resolution of the image data used in this study, the hard classifiers seem to be sufficient. If hyperspectral imagery with lower spatial resolution, such as 20-m AVIRIS data, is to be used, MTMF and other spectral unmixing techniques can be used to separate giant reed from mixed pixels. Image classification results depend on the composition and similarity of plant species and the growth conditions at a specific site, and the best classification methods identified for one giant reed site may not perform the best at other infested sites. Therefore, it is always a good practice to use two or more classifiers for image classification.

4. Conclusions

This study evaluated airborne hyperspectral imagery and compared six commonly used classifiers for distinguishing giant reed. Among the six classifiers examined,

SVM and ML generally performed better than the other four classifiers for distinguishing this invasive weed. Because of the variations in plant growth and ground cover conditions within classes, it is necessary to define subclasses within any non-uniform major classes (i.e. giant reed) for supervised classification.

Previous studies have demonstrated that aerial photography, airborne multi-spectral imagery and high resolution satellite imagery can all be used for mapping giant reed infestations using the ML classifier. Although there is no report on the use of SVM for detecting giant reed from multispectral imagery, both the SVM and ML classifiers can be used to classify multispectral and hyperspectral imagery. As more remote sensing imagery is becoming available, accuracy and cost associated with different types of imagery should be considered. Airborne multispectral imagery is generally cheaper to acquire and easier to process than hyperspectral imagery, so it is more cost-effective for this application. High resolution satellite imagery may be more effective than airborne imagery if large areas need to be mapped. Hyperspectral imagery requires more sophisticated camera systems and involves intensive data processing, but it has the potential to improve classification results if spectrally similar vegetation species to giant reed occur in the target imaging areas. Therefore, the type of imagery to be selected for a particular study depends on image availability, complexity of associated plant communities, size of the area, and time and cost constraints. More research is needed to compare different types of imagery for the detection of giant reed in terms of accuracy, suitability and cost-effectiveness.

Acknowledgements

The authors wish to thank Michael Ohlinger of Sterling Air Service at Weslaco, TX and Fred Gomez of USDA-ARS at Weslaco, TX for taking the hyperspectral imagery for this study and Jim Forward of USDA-ARS at Weslaco, TX for assistance in image rectification and ground verification.

References

- Bell, G.P., 1997. Ecology and management of *Arundo donax* and approaches to riparian habitat restoration in southern California. In: J.H. Brock, M. Wade, P. Pysek, and D. Green, eds. *Plant invasion studies from North America and Europe*. Leiden, the Netherlands: Blackhuys Publishers, 103–113.
- Cleere, G., 2007. A battle at the border: coping with Carrizo cane [online]. *Journal of Homeland Security*. Available from: <http://www.homelandsecurity.org/journal/Default.aspx?oid=154&ocat=1> [Accessed 22 August 2011].
- Congalton, R.G. and Green, K., 1999. *Assessing the accuracy of remotely sensed data: principles and practices*. Boca Raton, FL: Lewis Publishers.
- DiPietro, D., Ustin, S.L., and Underwood, E., 2002. Mapping the invasive plant *Arundo donax* at Camp Pendleton Marine Base using AVIRIS. In: *Proceedings of 10th JPL airborne visible infrared imaging spectrometer (AVIRIS) Workshop*, Pasadena, CA: Jet Propulsion Lab.
- Dudley, T.L., 2000. *Arundo donax*. In: C.C. Bossard, J.M. Randal, and M.C. Hosovsky, eds. *Invasive plants of California wildlands*. Berkeley, CA: University of California Press, 53–58.
- ERDAS, 2002. *ERDAS field guide*. Atlanta, GA: ERDAS LLC.
- Everitt, J.H., et al., 2004. Canopy spectra of giant reed and associated vegetation. *Journal of Range Management*, 57, 561–569.
- Everitt, J.H., Yang, C., and Deloach, C.J., 2005. Remote sensing of giant reed with QuickBird satellite imagery. *Journal of Aquatic Plant Management*, 43, 81–84.
- Everitt, J.H., et al., 2008. Comparison of QuickBird and SPOT 5 satellite imagery for mapping giant reed. *Journal of Aquatic Plant Management*, 46, 77–82.

- Glenn, N.F., *et al.*, 2005. Hyperspectral data processing for repeat detection of small infestations of leafy spurge. *Remote Sensing of Environment*, 95, 399–412.
- Green, A.A., *et al.*, 1988. A transformation for ordering multispectral data in terms of image quality with implications for noise removal. *IEEE Transactions on Geoscience and Remote Sensing*, 26, 65–74.
- Harsanyi, J.C. and Chang, C.I., 1994. Hyperspectral image classification and dimensionality reduction: an orthogonal subspace projection approach. *IEEE Transactions on Geoscience and Remote Sensing*, 32, 779–785.
- Hsu, C.-W., Chang, C.-C., and Lin, C.-J., 2007. *A practical guide to support vector classification*. Taipei, Taiwan: National Taiwan University.
- Iverson, M.E., 1994. The impact of *Arundo donax* on water resources. In: N.E. Jackson, P. Frandsen, and S. Douthit, eds. *Arundo donax workshop proceedings*, Ontario, Canada.
- Khudamrongsawat, J., Tayyar, R., and Holt, J.S., 2004. Genetic diversity of giant reed (*Arundo donax*) in the Santa Ana River, California. *Weed Science*, 52, 395–405.
- Kruse, F.A., *et al.*, 1993. The spectral image processing system (SIPS): interactive visualization and analysis of imaging spectrometer data. *Remote Sensing of Environment*, 44 (2–3), 145–163.
- Miao, X., *et al.*, 2006. Estimation of yellow starthistle abundance through CASI-2 hyperspectral imagery using linear spectral mixture models. *Remote Sensing of Environment*, 101, 329–341.
- Mundt, J.T., *et al.*, 2005. Discrimination of hoary cress and determination of its detection limits via hyperspectral image processing and accuracy assessment techniques. *Remote Sensing of Environment*, 96, 509–517.
- Narumalani, S., *et al.*, 2006. A comparative evaluation of ISODATA and spectral angle mapping for the detection of saltcedar using airborne hyperspectral imagery. *Geocarto International*, 21 (2), 59–66.
- Narumalani, S., *et al.*, 2009. Detecting and mapping four invasive species along the floodplain of North Platte River, Nebraska. *Weed Technology*, 23 (1), 99–107.
- Newhouser, M., Cornwall, C., and Dale, R., 1999. *Arundo: a landowner handbook*. Sacramento, CA: Sonoma Ecology Center and California State University, 22.
- Oakins, A.J., 2001. *An assessment and management protocol for Arundo donax in the Salinas Valley Watershed*. Thesis (MS). Monterey Bay, CA: California State University, 50.
- Parker-Williams, A.P. and Hunt, E.R. Jr., 2002. Estimation of leafy spurge cover from hyperspectral imagery using mixture tuned matched filtering. *Remote Sensing of Environment*, 82, 446–456.
- Richards, J.A., 1999. *Remote sensing digital image analysis*. Berlin: Springer-Verlag.
- Underwood, E., Ustin, S., and DiPietro, D., 2003. Mapping nonnative plants using hyperspectral imagery. *Remote Sensing of Environment*, 86, 150–161.
- Yang, C. and Everitt, J.H., 2007. Evaluating airborne hyperspectral imagery for mapping waterhyacinth infestations. *Journal of Applied Remote Sensing*, 1, 013546.
- Yang, C. and Everitt, J.H., 2010. Comparison of hyperspectral imagery with aerial photography and multispectral imagery for mapping broom snakeweed. *International Journal of Remote Sensing*, 31 (20), 5423–5438.
- Yang, C., Everitt, J.H., and Goolsby, J.A., 2011. Using aerial photography for mapping giant reed infestations along the Texas-Mexico portion of the Rio Grande. *Invasive Plant Science and Management*, 4 (4), 402–410.
- Yang, C., Everitt, J.H., and Johnson, H.B., 2009a. Applying image transformation and classification techniques to airborne hyperspectral imagery for mapping Ashe juniper infestations. *International Journal of Remote Sensing*, 30 (11), 2741–2758.
- Yang, C., Goolsby, J.A., and Everitt, J.H., 2009b. Using QuickBird satellite imagery to estimate giant reed infestations in the Rio Grande Basin of Mexico. *Journal of Applied Remote Sensing*, 3, 033530.
- Yang, C., *et al.*, 2003. A CCD camera-based hyperspectral imaging system for stationary and airborne applications. *Geocarto International Journal*, 18, 71–80.